Ceramics International 44 (2018) 13773–13781

Contents lists available at ScienceDirect

Ceramics International

journal homepage: www.elsevier.com/locate/ceramint

$La_{0.8}Sr_{0.2}Ga_{0.8}Mg_{0.2}O_3$ electrolytes prepared by vacuum cold spray under heated gas for improved performance of SOFCs

Li-Shuang Wang, Cheng-Xin Li*, Kai Ma, Shan-Lin Zhang, Guan-Jun Yang, Chang-Jiu Li

State Key Laboratory for Mechanical Behavior of Materials, School of Materials Science and Engineering, Xi'an Jiaotong University, Xi'an, Shaanxi Province 710049, PR China

ARTICLE INFO

Keywords:
Vacuum cold spray
Heated gas
LSGM
IT-SOFCs

ABSTRACT

High impact velocity of particles has found its common way into the vacuum cold spray (VCS), but heating gas may further intensify this function, resulting in significantly higher impact velocity. That's the original design idea to realize denser ceramic deposition at low temperature in this paper. In this study, a ~ 10 μm thick $La_{0.8}Sr_{0.2}Ga_{0.8}Mg_{0.2}O_3$ (LSGM) electrolyte layer for SOFCs is prepared by VCS under heated gas. The effects of gas temperature on the deposition behavior, mechanical and electrical properties of the coatings are investigated. Results show improvements in coating density, hardness and ionic conductivity at elevated temperature. Additionally, the output performance of cell with LSGM electrolytes deposited at gas temperature of 400 °C achieved an open circuit voltage of ~ 1.0 V and the maximum power density of 855 mW/cm^2 at 750 °C. Overall, these findings testify of the promising aspects of VCS method for preparing solid electrolyte films for IT-SOFCs.

1. Introduction

Solid oxide fuel cells (SOFCs) are electrochemical devices, which directly convert chemical energy into electricity. SOFCs are considered promising candidates for the next generation energy conversion systems, owing to their high energy conversion efficiencies and low environmental impacts [1,2]. For commercialization of SOFCs, research and development are mainly focused on lowering the operating temperature from 800–1000 °C to 600–800 °C. Intermediate-temperature SOFCs (IT-SOFCs) provide many advantages, including the use of inexpensive metal interconnectors, improvement in sealing abilities, and long-term operation stabilities. However, the conductivity of traditional yttria-stabilized zirconia (YSZ) solid electrolyte materials rapidly decrease at operating temperatures lower than 800 °C [2,3].

Doped lanthanum gallate (LSGM) materials have excellent ionic conductivities (~ 0.1 S/cm at 800 °C) and negligible electronic conductivities at reduced temperatures [4,5]. Furthermore, they present high chemical stabilities over a broad range of oxygen partial pressures (10^{-22} ~ 1 atm). Therefore, LSGM materials are good alternative candidate electrolyte materials for IT-SOFCs.

To fabricate LSGM electrolytes with dense microstructures suitable for SOFCs, the sintering temperatures should be above 1400 °C, where LSGM reacts with NiO-cermet anode and some perovskite cathode material [6–9]. The formation of reaction products with high resistance at the anode/electrolyte or cathode/electrolyte interfaces would significantly decrease the cell performance. On the one hand, the fabrication temperature of LSGM should be reduced to suppress the formation of secondary phases. Some studies reported that the sintering temperature of VCS LSGM coatings would decrease to 1200 °C by two-step densification processes [10]. On the other hand, LSGM solid electrolytes should achieve sufficient densities and could be deposited as thin film electrolytes to decrease the ohmic resistance and operating temperature.

Several deposition methods have been used to prepare LSGM thin films without high-temperature sintering processes. These include pulsed laser deposition (PLD) [11,12] and magnetron sputtering [13]. For instance, Hwang et al. systematically investigated the difficulties in preparing LSGM electrolyte thin films by PLD and succeeded in preparing high-quality LSGM thin films by optimizing target composition and substrate temperature [12]. The cell achieved excellent output performance with a maximum power density of ~ 1.1 W/cm^2 at 600 °C. Wang et al. prepared high-quality LSGM films with post-annealing at 1000 °C using RF magnetron sputtering [13]. The cell reached a maximum power density of ~ 1.38 W/cm^2 at 800 °C. However, the studies which have succeeded to achieve LSGM thin films with high quality are limited, because the stoichiometry and phase structure of the complex oxides are difficult to control by PLD or sputtering method. Besides, the low deposition rates and high manufacturing cost limit these methods

* Corresponding author.
E-mail address: licx@mail.xjtu.edu.cn (C.-X. Li).

https://doi.org/10.1016/j.ceramint.2018.04.220
Received 26 February 2018; Received in revised form 25 April 2018; Accepted 25 April 2018
Available online 26 April 2018

for large-scale SOFCs manufacturing. Therefore, the development of LSGM fabrication processes with high deposition rates and low deposition temperatures remain highly desirable.

Vacuum cold spray (VCS), which is also known as an aerosol deposition method (ADM), is used for ceramic film deposition. Compared to other ceramic film deposition techniques, VCS is advantageous in terms of high deposition rate and low deposition temperature. VCS is based on impact and adhesion of fine ceramic particles, yielding high deposition rates. Akedo et al. obtained deposition rates ranging from several micrometers to tens of micrometers during deposition of zirconate titanate (PZT) powders [14]. Also, the ceramic films could be deposited at low temperatures with no phase transformation during VCS process [15,16]. Additionally, VCS could be employed to achieve ceramic films with thicknesses less than 20 μm due to the use of nano-or micro-sized spray powders as feedstock. Therefore, VCS can be adopted to prepare LSGM thin electrolyte layers for SOFCs.

In cold spray (CS), the successful bonding of metal particles by impact results from plastic deformation and adiabatic shear instability occurring at high impact velocity [17,18]. Though the deposition mechanism of VCS remains unclear, the kinetic energy of the particles would highly contribute to the fracture and bonding between particles. Therefore, for both CS and VCS, the impact velocities between particles affect the microstructure and density of the resulting coatings. The impact velocity between particles depends mainly on particle size, powder agglomeration, process gas pressure and gas temperature, and nozzle geometry [15,19–22]. The increase in gas temperature would effectively improve the coating density in VCS and particle impact velocity. Furthermore, in-situ particle heating could be achieved by increasing gas temperature during VCS processes. Yao et al. fabricated TiO_2 films by VCS [23], and found that particle connection and electronic conductivity were improved through in-situ particle heating during the VCS process.

In this study, the effects of gas temperature on the mechanical and electrical properties of VCS LSGM films were examined. The carrier gas was preheated to different temperatures of 200 °C and 400 °C, respectively. For comparative purposes, the VCS LSGM film without carrier gas heating (e.g., 25 °C) was also prepared and tested under the same conditions. The gas temperature was optimized and SOFCs were assembled to yield improved VCS LSGM electrolyte films suitable for SOFCs applications.

2. Experimental

2.1. Materials preparation and characterization

Commercially available $La_{0.8}Sr_{0.2}Ga_{0.8}Mg_{0.2}O_3$ (LSGM) (Fuelcellmaterials, USA) was used as the starting powder. Before deposition, the LSGM powders were completely dried in a furnace at 120 °C. For anode preparation, NiO and YSZ powders were mixed at 5:5 volume ratio, as described elsewhere [24]. The anode powder was then pressed into pellets at 240 MPa and pre-sintered at 1100 °C. To prevent diffusion of Ni towards the LSGM electrolyte layer, $Gd_{0.1}Ce_{0.9}O_{1.95}$ (GDC) buffer layer with thickness of 2–3 μm was coated preferentially on NiO-YSZ substrate using the tape casting method. The NiO-YSZ/GDC double layers were then co-sintered at 1300 °C. In addition, c-plane sapphier (1000) substrate was used for the electrical and mechanical tests.

The morphologies and phase structures of the LSGM powders were analyzed by scanning electron microscopy (SEM, TESCAN MIRA 3 LMH, Czech Republic)) and X-ray diffraction (XRD, Shimadzu XRD-6000, Kyoto, Japan) with Cu-K_α radiation.

2.2. Preparation and characterization of LSGM coatings

LSGM coatings were deposited by VCS-2000 vacuum cold spray system developed at the Xi'an Jiaotong University. The system consisted of vacuum chamber, aerosol chamber, carrier gas feeding unit, particle-accelerated nozzle, and three-dimensional worktable. The detailed equipment was described elsewhere [25,26]. At chamber pressures lower than 1000 Pa, the dried LSGM powders were mixed with the carrier gas to form an aerosol flow in the aerosol chamber. The particles were further accelerated through a Laval nozzle after injection of the aerosol flow into the vacuum chamber. The LSGM film was formed on the substrate by moving the nozzle. After injection into the vacuum chamber, the aerosol flow was heated by a hot pipe at controlled temperatures of 200 °C and 400 °C, respectively. Besides, the aerosol flow without heat treatment was also employed for comparison. The surface and cross-sectional morphologies of the LSGM films deposited at different temperatures were characterized by SEM and phase structure was determined by XRD.

To reveal the deposition behaviors, the deposition units at different deposition temperatures were collected by scanning through the substrate in one pass at nozzle traversal speed of 20 mm/s. The microstructure of the deposition unit was characterized by SEM.

2.3. Electrical and mechanical characterization

Electrochemical impedance spectroscopy (EIS) (Solartron SI 1260/1287 impedance analyzer) combined with AC two probe method was employed to measure the difference in the electrical conductivity of LSGM thin films deposited at different temperatures on sappier substrates. The electrode configuration is shown in Fig. 1. Silver pastes painted on LSGM film surfaces with distances of 2 mm were used as the electrodes. The silver coated samples were then fired at 200 °C for 2 h to ensure better adhesion between the samples and the electrodes. The conductivities of different LSGM thin films were measured from 500 °C to 750 °C. During testing, the frequency varied from 10^{-1} to 10^5 Hz at applied AC voltage of 25 mV.

The mechanical properties of different LSGM films were characterized by TI950 TriboIndenter (Hysitron, Minneapolis, MN) with a standard Berkovich indenter at room temperature. The hardness (H) and elastic modulus (E) were obtained from the load-displacement curve of Berkovich indenter. At least 10 indentations were made on different zones for each sample.

2.4. Comparison of VCS-LSGM electrolyte-based SOFCs performances

After deposition of LSGM films on anode substrates, LSCF cathodes with thicknesses of 20–30 μm were prepared by screen-printing method followed by sintering at 1080 °C for 2 h [10]. After reduction of NiO to Ni in the H_2 atmosphere at 700 °C for 2 h, the performances of single cells were tested in a furnace at heating and cooling rates of 3 °C/min. Air (0.15 slpm) and humidified H_2 with 3% H_2O (0.1 slpm) were utilized as the oxidant and fuel, respectively. The operating temperature was varied from 600 °C to 750 °C at an interval of 50 °C and current-voltage-power curves (V-I and P-I) were obtained at each temperature.

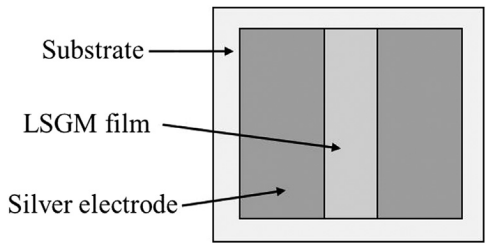

Fig. 1. Electrode configuration of AC two probe method.

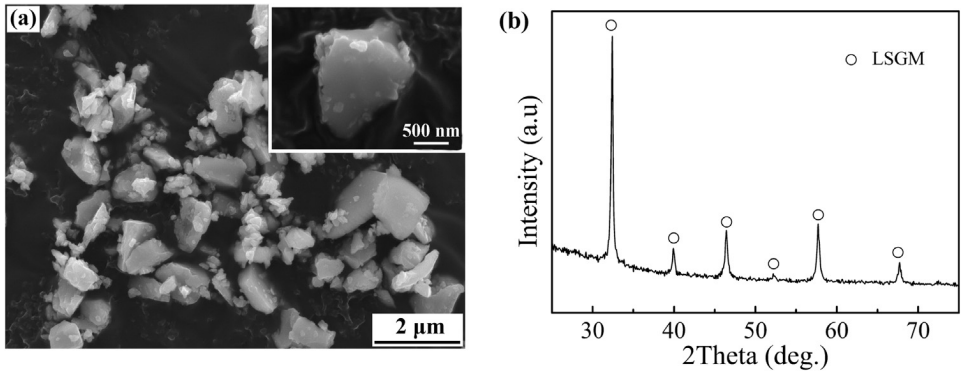

Fig. 2. (a) Morphologies of LSGM starting powders, and (b) XRD pattern of LSGM starting powders. The inset in (a) shows the high magnified image.

3. Results and discussion

3.1. Phase structures of LSGM films deposited at different gas temperatures

Fig. 2 shows the morphologies and phase structures of the starting powders. The powders exhibited angular morphologies with an average particle size of ~ 1.5 μm (see Fig. 2a). Also, the powders had single perovskite structures without the presence of secondary phases (see Fig. 2b). After being dried, these powders were used to deposit LSGM coatings. The deposition parameters are listed in Table 1.

Fig. 3 shows the XRD patterns of LSGM films deposited at 25 °C (R.T), 200 °C and 400 °C, respectively. As shown in Fig. 3a, all the LSGM films showed perovskite structures, which was identical to those of original powders (see Fig. 2b), indicating that no phase transformation occurred during the VCS process. As shown in Fig. 3b, broadening of the spectra combined with slight shifting of the peaks appeared as gas temperature rose, suggesting a decrease in crystalline size. This characteristic was typical of films prepared by VCS. For example, vacuum cold spraying of ceramic powders (e.g., Al_2O_3, YSZ [27], $Li_7La_3Zr_2O_{12}$ [28], and Gd-doped ceria [16]) induced broadened spectra with shifted peaks of the XRD patterns. This was attributed to fragmentation of the particles during collision with the substrate. The film deposited at 400 °C showed the widest peaks or largest full-width half maximum (FWHM) values, indicating films with smallest crystallite sizes. Therefore, LSGM particles became severely fractured as the aerosol temperature rose during VCS process.

3.2. Microstructure of LSGM films deposited at different temperatures

As a beforehand work, deposition unit, which is the basic unit to form the coating, was used to investigate the deposition behavior of LSGM during VCS process. The deposition unit can be collected by quickly scanning the sappier substrate with one pass following the same parameters as those used for the coating deposition [26,29]. Typical morphologies of the deposition units obtained under different gas temperature are shown in Fig. 4. Fig. 4a indicates that the particle deposited at room temperature was similar to the original powders (see Fig. 2a), except of the new-formed cracks observed on the surface. The cracks propagated from one side to the middle of the particle. In terms of the case deposited at 200 °C, as shown in Fig. 4b, it can be seen that the particle became flattened, along with some wider cracks with respect to the case deposited at room temperature (see Fig. 4a). In addition, the particle was divided approximately into two parts, suggesting that the crack run through the particle. In terms of the case deposited at 400 °C, as shown in Fig. 4c, it is found that more cracks were formed and propagated randomly, dividing the flattened particle into several parts. Therefore, the flattening and cracking of the particles strengthened as the aerosol temperature rose.

Table 1
Deposition parameters for vacuum cold spraying.

Parameter	Value	Unit
Chamber pressure	150	Pa
Pressure in powder unit	10	KPa
He gas flow rate	3.5	L min^{-1}
Distance from nozzle exit to substrate	5	mm
Nozzle traversal speed	2	mm s^{-1}
Gas temperature	25, 200, 400	°C

In brief, different deposition behaviors of LSGM particles among different gas temperatures are schematically described in Fig. 5. At 25 °C, slight fracture of LSGM particles occur when they collide on the substrate (see Fig. 5a), which means that the particle would be relatively intact. After being consolidated by the following particles, large gaps between particles still exist between fragments. At 200 °C, the LSGM particles are fractured and subjected to plastic deformation upon impact on the substrate (see Fig. 5b). The resulted size of fragment is decreased and the corresponding gaps are narrowed after being consolidated. At the gas temperature of 400 °C, severe fracture and deformation occur after LSGM particles are impacted on the substrate. After being consolidated by the following particles, the resulted size of fragment is further decreased, and the lower layers would thereby seem to be denser.

The polished cross-sectional microstructures of LSGM coatings at different gas temperatures are shown in Fig. 6. These coatings were deposited using layer by layer process. In the case of deposition at room temperature, as shown in Fig. 6a and d, the coating appeared to be porous with clear gaps between particles. These gaps were resulted from the partial fracture of individual particles (see Fig. 4a and Fig. 5a) during deposition process. When the gas temperature was increased to 200 °C, the LSGM film became denser, yet a few pore-like interfaces between particles can still be observed (see Fig. 6b and e). The flatness and fracture of the particles enhanced the particle bonding (see Fig. 4b and Fig. 5b). In the case of deposition at 400 °C, the coating was further densified (see Fig. 6c and f). As a result, the particle/particle interfaces were difficult to observe due to severe fragmentation and deformation of particles (Fig. 4c and Fig. 5c). This improved significantly the particle bonding.

The effect of gas temperature on the difference in deposition behaviors and microstructure can be attributed to two aspects. On the one hand, higher gas temperature would lead to the increase in particle velocity during vacuum cold spray, when particles were accelerated in the nozzle. This is consistent with the investigation on cold spray [19,30,31]. Consequently, the high impact velocities would result in severe fragmentation and deformation of particles, since more kinetic energy was converted to fracture and deformation energies. Chun et al. reported that fragments would stick together with weak bonding during deposition [32]. The following particles with high impact velocity would then consolidate these fragmentations through filling the

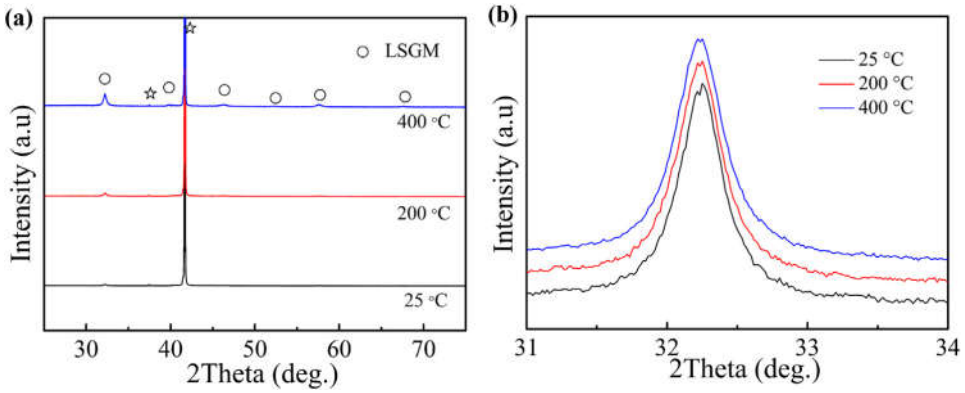

Fig. 3. XRD patterns of LSGM deposited at different gas temperatures in the 2θ range of: (a) 25–75° and (b) 31–34°. (☆: sapphire substrate).

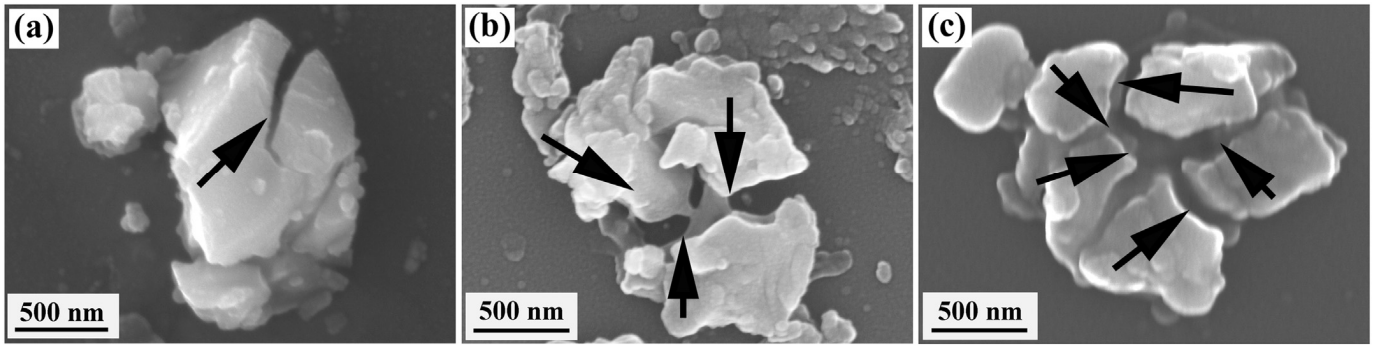

Fig. 4. Typical morphologies of LSGM deposited at different gas temperatures: (a) 25 °C, (b) 200 °C, and (c) 400 °C. The black arrows correspond to the fractured regions.

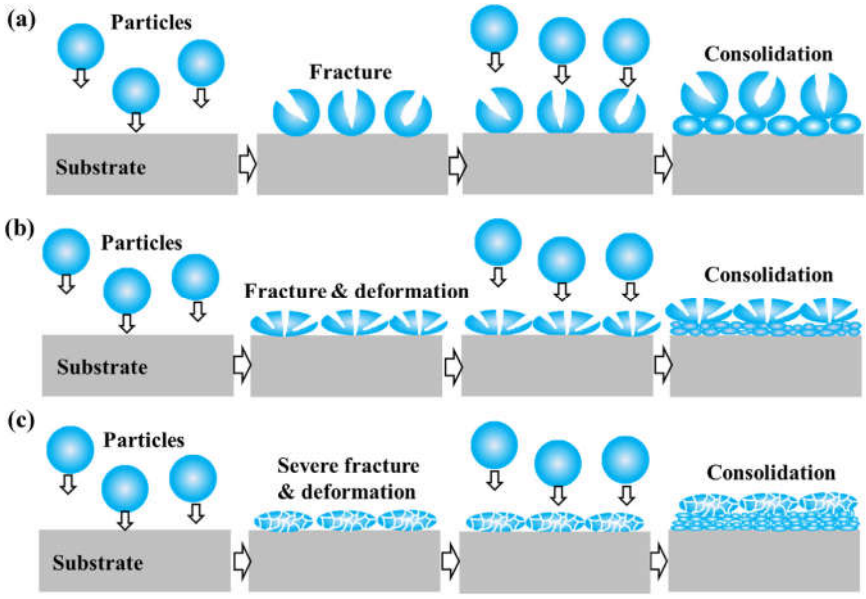

Fig. 5. Schematic representation of behavior of LSGM particles deposited at different gas temperatures: (a) 25 °C, (b) 200 °C, and (c) 400 °C.

interstices, and by tampering effect as well. On the other hand, high gas temperature softens the ceramic particles, hence enabling easier particle deformation [33]. This can be responsible for the formation of denser VCS LSGM coatings when the gas temperature is increased.

3.3. Electrical properties

Fig. 7 illustrates the conductivity of LSGM thin films deposited at different aerosol temperatures. The film conductivity increased as gas temperature rose. The films deposited at 200 °C and 400 °C showed high conductivities of 0.028 S/cm and ~ 0.043 S/cm at 750 °C, respectively. However, the conductivity significantly decreased to 0.003 S/cm when the film was deposited at 25 °C. The large difference in conductivity may be related to the microstructures of LSGM films. At low temperature, partial fracture of particles occurred and particle interface bonding weakened in the film (see Fig. 4a, Fig. 6a and d). This limited oxygen ion transfer and decreased the ionic conductivity. As gas temperature increased to 200 °C, the particles flattened and fractured to

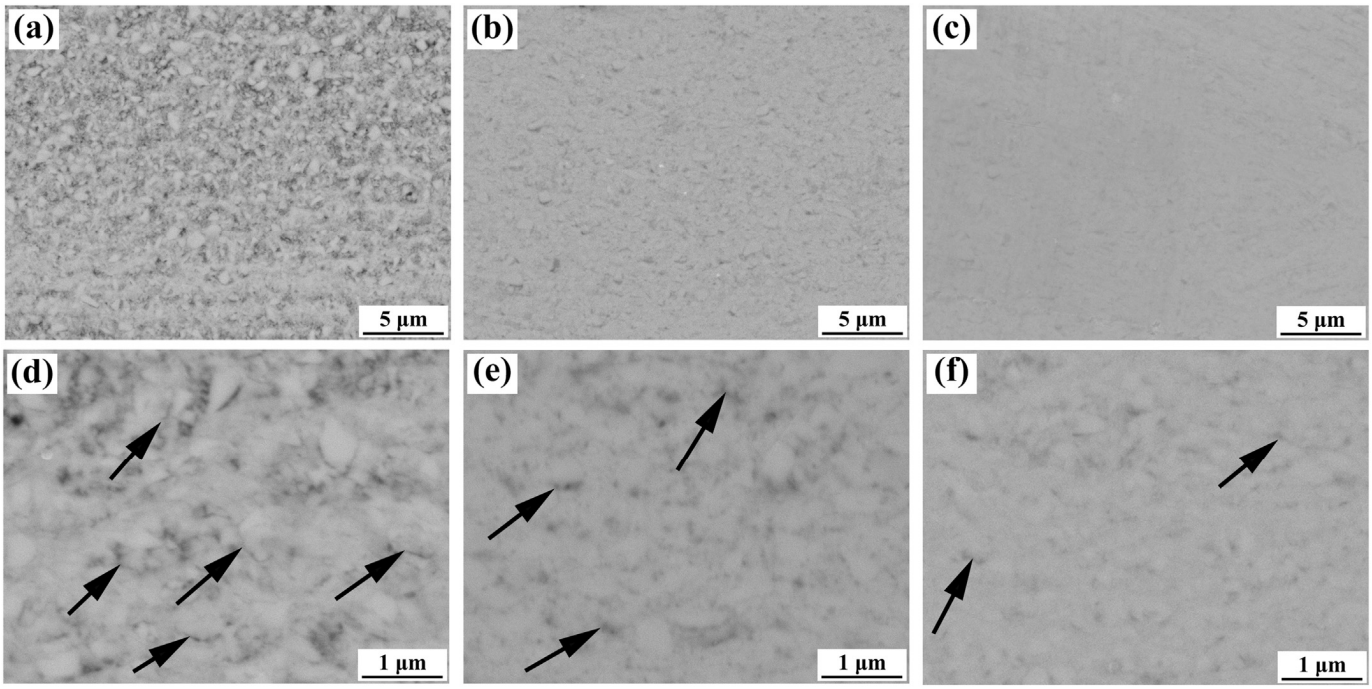

Fig. 6. Polished cross-sectional microstructures of VCS LSGM films deposited at different gas temperatures: (a, d) 25 °C, (b, e) 200 °C, and (c, f) 400 °C. (a, b, c) represent the low magnified images and (d, e, f) high magnified images. The black arrows correspond to the particle/particle interface.

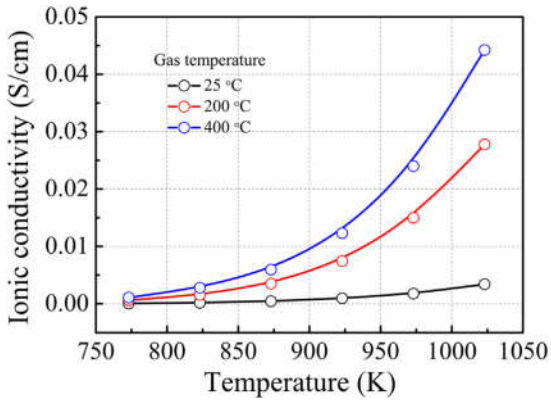

Fig. 7. Ionic conductivity of LSGM coatings deposited at different gas temperatures.

several parts upon impact with the substrate (see Fig. 4b), and particle/particle interface bonding improved (see Fig. 6b and e). The film fabricated by VCS process was based on collision and adhesion of particles, making strong particles bonding to improve film conductivity. At gas temperature of 400 °C, the large impact velocities of particles enhanced particle bonding (see Fig. 4c, Fig. 6c and f), resulting in films with large conductivities.

Chun et al. reported that shock compaction effect based on consolidation of subsequent particles as an essential phenomenon allowing ceramic particles bonding during VCS [32]. The shock compaction of ceramic particles would include powder particle fragmentation, pores filling and particle surface heating, and melting or element diffusion [34]. Additionally, explosive liquid phase sintering may occur upon impaction due to slow dissipation of thermal energy, leading to welding of neighbour powder particles [35]. Here, plastic deformation and fragmentation occurred during VCS process (Fig. 4 and Fig. 5). Therefore, bonding of particles was induced from shock compaction of LSGM particles. The high ionic conductivities of LSGM coatings probably induced excellent particle/particle interface bonding for particles deposited at high gas temperatures due to large kinetic energies. In other words, defects like gaps or pores in LSGM coatings decreased as gas temperature rose.

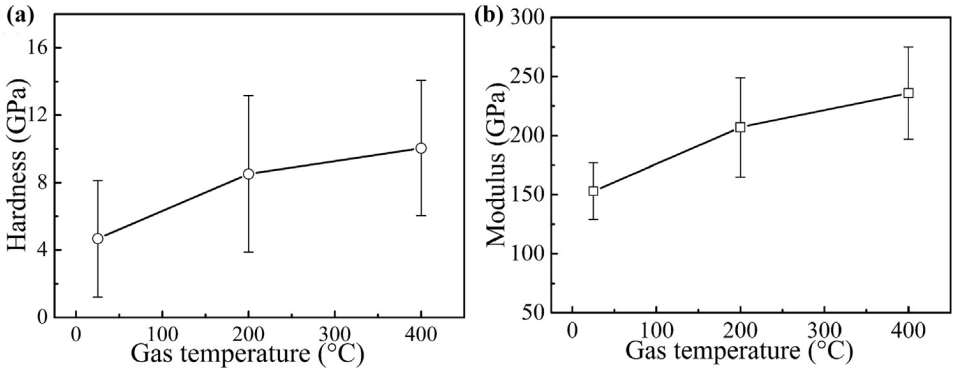

Fig. 8. Hardness and elastic modulus of coatings deposited at different gas temperatures.

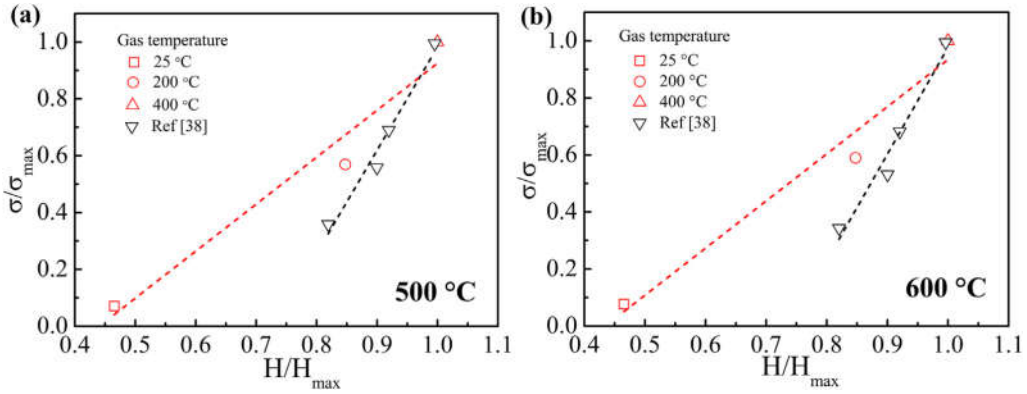

Fig. 9. $\sigma/\sigma ma_x$ vs. H/H_{max} of LSGM coatings at different operation temperatures: (a) 500 °C and (b) 600 °C. Black symbols and the fitting line correspond to the data taken from Ref. [38].

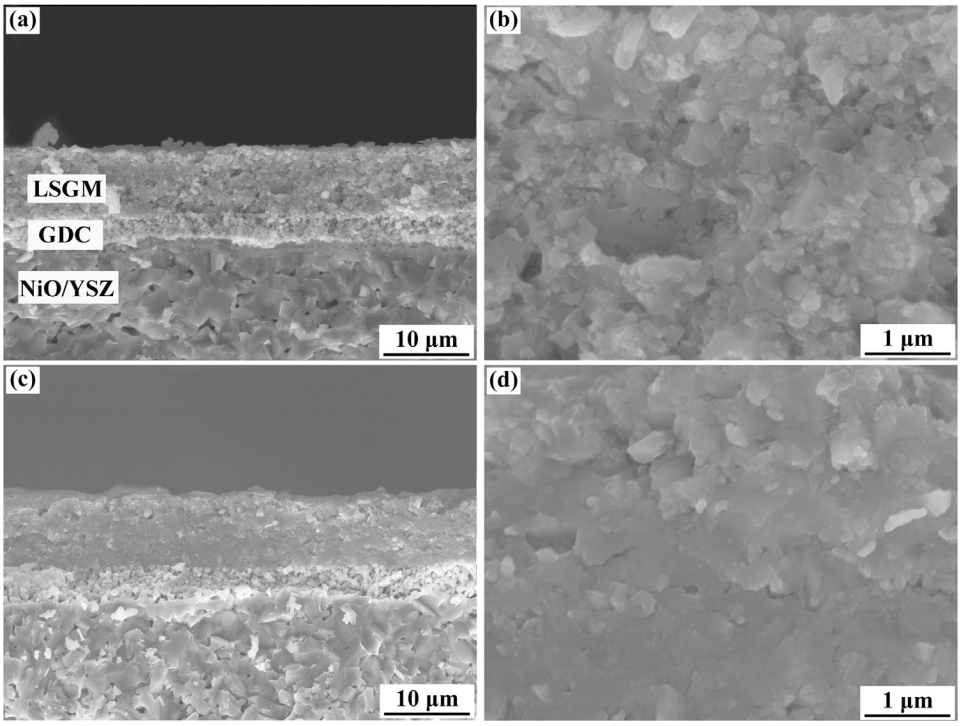

Fig. 10. Fractured cross-sectional morphologies of LSGM deposited on anode substrates at different gas temperatures: (a, b) 200 °C and (c, d) 400 °C. (a, c) represent the low magnified images and (b, d) high magnified images.

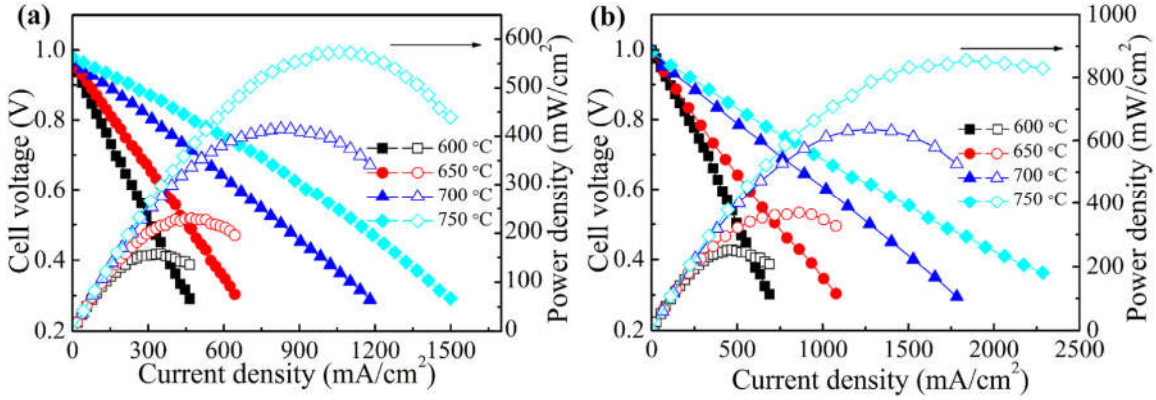

Fig. 11. Output performance of SOFCs assembled with VCS LSGM coatings deposited at different gas temperatures: (a) 200 °C and (b) 400 °C.

Table 2
MPD of two types of cells operating at different temperatures.

Operating temperature (°C)	MPD (mW/cm^2)	
	Cell A	Cell B
600	157	252
650	230	370
700	415	636
750	573	855

3.4. Mechanical properties

Fig. 8 depicts the hardness and modulus values of VCS LSGM coatings deposited at different gas temperatures. Both hardness and modulus values rose with gas temperature. The average hardness and modulus values at (400 °C, 200 °C, and 25 °C) were recorded as (~ 10.5, 8.5, and 4.7 GPa) and (236, 207, and 153 GPa), respectively. Li et al. reported that microstructures of thermal spray coatings significantly affected their mechanical properties [36]. Chun et al. suggested that improved hardness and modulus values of VCS Al_2O_3 coatings were due to enhanced ceramic particles bonding [32]. On the other hand, VCS Al_2O_3 coatings with strong particle/particle bonding would have higher hardness [26]. Therefore, as gas temperature rose, the LSGM coatings showed better particle interface bonding. These results were consistent with microstructures of LSGM coatings (see Fig. 4 and Fig. 6). At gas temperature of 400 °C, the average hardness and modulus values were ~ 10.5 GPa and 236 GPa, respectively. These values were slightly lower than those of sintered LSGM bulk reported by others [37,38]. Morales and his co-authors found that hardness was influenced by relative density and purity of LSGM samples [38]. Here, the relative density of LSGM coatings affected hardness and modulus due to their pure perovskite structures without the presence of secondary phases (see Fig. 3). Therefore, the relative density of LSGM coatings increased with gas temperature. Morales et al. mentioned that sintered $La_{0.9}Sr_{0.1}Ga_{0.8}Mg_{0.2}O_{3-\delta}$ with density of ~ 95% and $La_{0.85}Sr_{0.15}Ga_{0.8}Mg_{0.2}O_{3-\delta}$ with density of ~ 98% had hardness values of ~ 11.25 GPa and ~ 13.14 GPa, respectively [38]. Compared to LSGM sintered bulk, lower hardness values of VCS LSGM coatings would mainly be attributed to low densities. Additionally, errors of H and E values obtained from VCS coatings were higher than those of SPS bulk samples. The reason for this had to do with surface roughness of VCS LSGM coatings, which was larger than that of polished sintered bulks. This was consistent with data reported by Chun et al. [32]. In their report, despite the optimized penetration depth in nano-indentation testing to improve precision, the errors of H and E values of VCS Al_2O_3 coatings were still larger than those of polished sintered bulks.

To clarify the relationship between the mechanical and electrical properties of VCS LSGM coatings, the σ/σ_{max} ratio was plotted against H/H_{max} ratio at different testing temperatures for VCS LSGM coatings deposited at different gas temperatures (see Fig. 9). For comparison, relevant data from the literature was added to Fig. 9. The H/H_{max} ratio represented the hardness (mechanical properties) of VCS LSGM coatings, while σ/σ_{max} ratio corresponded to their ionic conductivities (electrical properties). The H values were obtained for different samples, where H_{max} represented the maximum value. Similarly, σ values were obtained for all samples, with σ_{max} as the maximum value. H_{max} and σ_{max} corresponded to hardness and ionic conductivity values of VCS LSGM coatings deposited at 400 °C, respectively. Fig. 9 revealed that σ/σ_{max} ratios were proportional to H/H_{max} ratios at the operation temperature of 500 °C and 600 °C. Therefore, the effects of microstructures on both the ionic conductivity and hardness were similar to each other. This was consistent with data reported by Morales et al. [38]. In their report, sintered $La_{0.9}Sr_{0.1}Ga_{0.8}Mg_{0.2}O_{3-\sigma}$ ceramics with different relative densities and phase compositions showed linear correlations between hardness and ionic conductivity. The LSGM coatings tested here had the same phase composition and showed different relative density (see Fig. 4). Therefore, the effects of coating relative densities on the electrical and mechanical properties were close.

3.5. Effect of gas temperature on cell output performance

The VCS LSGM coatings deposited at gas temperatures of 200 °C and 400 °C (named as coating A and B, respectively) were selected for cell assembly because the coatings deposited at room temperature had porous microstructures and low mechanical properties. The LSGM electrolyte coatings were first deposited on anode substrates at 200 °C and 400 °C. The fractured cross-sectional morphologies of the resulting LSGM electrolyte films are shown in Fig. 10. The SEM images at low magnification revealed that half-cells were mainly composed of NiO/YSZ anode layer, GDC buffer layer, and LSGM electrolyte layer, respectively (see Fig. 10a and c). The thickness of both LSGM electrolytes was ~ 10 μm. Besides, a visible interface bonding can be observed in LSGM/GDC. Coating A seemed denser than coating B. The magnified SEM images indicated that fragmentation and deformation of particles occurred during VCS process (see Fig. 10b and d). Improved particle/particle interface bonding was observed in the cross-sectional images of coating B. Besides, the grain size of coating A was larger than that of coating B, indicating that severe fragmentation of particles occurred at high gas temperatures. The latter was consistent with the data discussed in Section 3.2.

After preparing LSCF cathodes by screen printing method, the cells were fired at 1080 °C to form porous cathode layers. The SOFC assembled with VCS LSGM electrolyte layers deposited at 200 °C and 400 °C were named as cell A and cell B, respectively. The output performances of the cells as a function of the operating temperature are gathered in Fig. 11. The maximum open circuit voltages (OCVs) of both cells were determined as ~ 0.98 V and ~ 1.0 V, respectively. The slightly lower OCV of cell A may be attributed to the different microstructure of LSGM coatings (see Fig. 10). Meanwhile, the maximum power density (MPD) of cell B was larger than that of cell A. The MPD values of both cells at various temperatures are summarized in Table 2. As the operating temperature rose, the MPD values significantly increased due to improved catalytic activity and ionic conductivity of the electrolyte. At 750 °C, the MPD of cell B was ~ 1.5-folds larger than that of cell A. The lower MPD values of cell A would mainly be attributed to

Table 3
Performance of LSGM electrolytes on Ni-based anode fabricated by spraying method in the literatures.

Cell sources	LSGM thickness (μm)	Fabrication method	Anode	Cathode	Temperature (°C)	Power density (W/cm^2)
This study	~ 10	VCS	NiO/YSZ-GDC	LSCF	750	0.855
Ref. [39]	~ 12	ADM	NiO/GDC	LSCF	750	1.18
Ref. [40]	~ 10	ADM	NiO/GDC	LSCF	750	0.79
Ref. [10]	~ 5	VCS + co-sintering	NiO/YSZ-GDC	LSCF	750	0.592
Ref. [41]	50–55	APS	NiO/YSZ-GDC	LSCF	750	0.502
Ref. [42]	~ 50	APS	NiO/LDC-LDC	SDC-SSC	750	0.716
Ref. [43]	50–60	APS	NiO/YSZ	LSCF	750	0.275
Ref. [44]	~ 60	APS	NiO/YSZ	LSCo	750	0.25

two reasons. On the one hand, the ionic conductivity of VCS LSGM electrolyte film deposited at 200 °C was lower than that deposited at 400 °C (see Fig. 7). Thus, the ohmic resistance of cell A was larger than that of cell B, resulting in lower MPD of cell A. On the other hand, as confirmed by XRD of Fig. 3 and magnified SEM images of Fig. 10, the smaller grain size of LSGM film deposited at 400 °C increased the specific surface area of the electrolyte layer of cell B. This resulted in more third phase boundaries (TPBs) at the electrolyte/cathode interface [10]. The power density of cell B was thus improved. Therefore, higher ionic conductivity of the electrolyte and more TPBs at electrolyte/cathode interface induced better output performance of cell B. The performances of SOFCs prepared by spray method are summarized in Table 3. The cell performance depended on LSGM electrolyte thickness. Atmospheric plasma spray (APS) is an costly and effective method to prepared components of SOFCs. The thickness of LSGM electrolyte coating prepared by APS was more than 50 μm, resulting in difficulty in further improvement of performance [41–44]. Using VCS (ADM), ~ 10 μm thick of LSGM electrolyte layers could be obtained, significantly improving cell performance. In our previous work, a double-layer design method for VCS prepared LSGM electrolyte assisted with two-step sintering at a low temperature was proposed [10]. The co-sintered LSGM with a thickness (~ 5 μm) was employed to assemble SOFC [10]. At 750 °C, the power density of cell was 0.592 W/cm^2, which is lower than that in the present study. On one hand, the SOFC assembled with co-sintered LSGM electrolyte layer presented a maximum open circuit voltage (OCV) of 0.956 V, which was a little lower than the OCV values of ~ 1.0 V in the present study. The lower OCV values may result in a low power density of cells. On the other hand, as reported by Kim and his co-authors, when the LSGM electrolyte and GDC buffer layer was co-fired at 1450 °C for 5 h, the reaction product $LaSrGa_3O_7$ phase with high resistance was formed [8]. Similarly, Hrovat et al. also observed the $LaSrGa_3O_7$ phase when the pellets of LSGM and GDC were co-fired at 1300 °C for 300 h [45]. Although the sintering temperature of VCS LSGM was decreased to 1200 °C, the interfacial reaction between LSGM and GDC was not completely avoided. The very few interfacial reaction products $LaSrGa_3O_7$ was detected in the LSGM/GDC interface. In the present study, a dense LSGM electrolyte layer was deposited by VCS at gas heating of 400 °C, which could completely avoid the interfacial reaction between LSGM and GDC. Therefore, in the present study, a higher power density was achieved. Here, the SOFC assembled with a VCS LSGM electrolyte layer achieved a maximum power density of 0.855 W/cm^2, which was acceptable for IT-SOFCs applications.

4. Conclusions

In the present study, LSGM electrolyte layers for SOFC were prepared by vacuum cold spray. During the spraying, carrier gas heating was employed to improve the particle interface bonding. The phase structures of VCS LSGM coatings with or without carrier gas heating were the same as the starting powders. The crystalline size was decreased with the increase of gas temperature. The effect of gas temperature on microstructure was investigated through particle impact behavior during the initial stages. For LSGM coatings deposited at room temperature, the particles were partially fractured. As temperature increased to 200 °C, the particles became deformed and fractured. As temperature further rose to 400 °C, the flattened particles were completely fractured into several parts. Therefore, the particle impact velocity improved as gas temperature rose, resulting in facilitated deformation and fragmentation of particles. At 750 °C, compared to LSGM coatings deposited at room temperature, the ionic conductivity of LSGM coatings deposited at 400 °C was increased more than tenfold. Similarly, the hardness was also increased from 4.7 GPa to 10.5 GPa. The improved electrical and mechanical properties of VCS LSGM films were achieved by carrier gas heating, mainly attributed to improved particle impact velocities. The linear relationship between ionic conductivity and hardness indicated that the electrical properties and mechanical properties of LSGM coatings may be controlled by the coating density (e.g., the particle/particle interface bonding). Therefore, the difference in microstructure yielded different mechanical and electrical properties, thus varied output performances of cells. In particular, the cells assembled with LSGM films deposited at 400 °C showed better output performances, with maximum power densities reaching up to 855 mW/cm^2 at 750 °C. The cell output performance can be further improved, such as optimizing electrode layer. Overall, vacuum cold spray under heated gas is a feasible way to prepare good quality LSGM electrolyte layer in SOFCs.

Acknowledgements

The work was supported by National Key R&D Program of China (Grant NO. 2017YFB0306100) and National Natural Foundation of China (Grant NO. 51761145108).

References

[1] O. Yamamoto, Solid oxide fuel cells: fundamental aspects and prospects, Electrochim. Acta 45 (15–16) (2000) 2423–2435.
[2] E. Ivers-Tiffee, A. Weber, D. Herbstritt, Materials and technologies for SOFC-components, J. Eur. Ceram. Soc. 21 (10–11) (2001) 1805–1811.
[3] E.C. Subbarao, H.S. Maiti, Solid electrolytes with oxygen ion conduction, Solid State Ion. 11 (4) (1984) 317–338.
[4] T. Ishihara, H. Matsuda, Y. Takita, Doped $LaGaO_3$ perovskite-type oxide as a new oxide ionic conductor, J. Am. Chem. Soc. 116 (9) (1994) 3801–3803.
[5] P.N. Huang, A. Petric, Superior oxygen ion conductivity of lanthanum gallate doped with strontium and magnesium, J. Electrochem. Soc. 143 (5) (1996) 1644–1648.
[6] M. Feng, J.B. Goodenough, K.Q. Huang, C. Milliken, Fuel cells with doped lanthanum gallate electrolyte, J. Power Sources 63 (1) (1996) 47–51.
[7] K.Q. Huang, M. Feng, J.B. Goodenough, C. Milliken, Electrode performance test on single ceramic fuel cells using as electrolyte Sr- and Mg-doped $LaGaO_3$, J. Electrochem. Soc. 144 (10) (1997) 3620–3624.
[8] K.N. Kim, B.K. Kim, J.W. Son, J. Kim, H.W. Lee, J.H. Lee, J. Moon, Characterization of the electrode and electrolyte interfaces of LSGM-based SOFCs, Solid State Ion. 177 (19–25) (2006) 2155–2158.
[9] K.Q. Huang, M. Feng, J.B. Goodenough, M. Schmerling, Characterization of Sr-doped $LaMnO_3$ and $LaCoO_3$ as cathode materials for a doped $LaGaO_3$ ceramic fuel cell, J. Electrochem. Soc. 143 (11) (1996) 3630–3636.
[10] L.S. Wang, C.X. Li, G.R. Li, G.J. Yang, S.L. Zhang, C.J. Li, Enhanced sintering behavior of LSGM electrolyte and its performance for solid oxide fuel cells deposited by vacuum cold spray, J. Eur. Ceram. Soc. 37 (15) (2017) 4751–4761.
[11] T. Ishihara, H. Eto, J.W. Yan, Intermediate temperature solid oxide fuel cells using $LaGaO_3$ based oxide film deposited by PLD method, Int. J. Hydrog. Energ. 36 (2) (2011) 1862–1867.
[12] J. Hwang, H. Lee, J.H. Lee, K.J. Yoon, H. Kim, J. Hong, J.W. Son, Specific considerations for obtaining appropriate $La_{(1-x)}Sr_{(x)}Ga_{(1-y)}Mg_yO_{(3-\delta)}$ thin films using pulsed-laser deposition and its influence on the performance of solid-oxide fuel cells, J. Power Sources 274 (2015) 41–47.
[13] S.F. Wang, H.C. Lu, Y.F. Hsu, Y.X. Hu, Solid oxide fuel cells with $(La,Sr)(Ga,Mg)O_{3-\delta}$ electrolyte film deposited by radio-frequency magnetron sputtering, J. Power Sources 281 (2015) 258–264.
[14] J. Akedo, M. Lebedev, Powder preparation in aerosol deposition method for lead zirconate titanate thick films, Jpn. J. Appl. Phys. 41 (11B) (2002) 6980–6984.
[15] S.M. Nam, N. Mori, H. Kakemoto, S. Wada, J. Akedo, T. Tsurumi, Alumina thick films as integral substrates using aerosol deposition method, Jpn. J. Appl. Phys. 1 (43) (2004) 5414–5418 (8A).
[16] H. Bae, J. Choi, G.M. Choi, Electrical conductivity of Gd-doped ceria film fabricated by aerosol deposition method, Solid State Ion. 236 (2013) 16–21.
[17] H. Assadi, F. Gartner, T. Stoltenhoff, H. Kreye, Bonding mechanism in cold gas spraying, Acta Mater. 51 (15) (2003) 4379–4394.
[18] M. Grujicic, C.L. Zhao, W.S. DeRosset, D. Helfritch, Adiabatic shear instability based mechanism for particles/substrate bonding in the cold-gas dynamic-spray process, Mater. Des. 25 (8) (2004) 681–688.
[19] T. Schmidt, F. Gartner, H. Assadi, H. Kreye, Development of a generalized parameter window for cold spray deposition, Acta Mater. 54 (3) (2006) 729–742.
[20] D.W. Lee, H.J. Kim, Y.H. Kim, Y.H. Yun, S.M. Nam, Growth process of α-Al_2O_3 ceramic films on metal substrates fabricated at room temperature by aerosol deposition, J. Am. Ceram. Soc. 94 (9) (2011) 3131–3138.
[21] H. Katanoda, M. Fukuhara, N. Iino, Numerical simulation on impact velocity of ceramic particles propelled by supersonic nitrogen gas flow in vacuum chamber, Mater. Trans. 48 (6) (2007) 1463–1468.
[22] K. Binder, J. Gottschalk, M. Kollenda, F. Gartner, T. Klassen, Influence of impact angle and gas temperature on mechanical properties of titanium cold spray deposits, J. Therm. Spray. Technol. 20 (1–2) (2011) 234–242.
[23] H.L. Yao, G.J. Yang, S. Li, X.L. He, S.Q. Fan, C.X. Li, C.J. Li, Synergistic effects of high temperature and impact compaction on the nano-TiO_2 film for the significant improvement of photovoltaic performance of flexible dye-sensitized solar cells, Electrochim. Acta 87 (2013) 940–947.

[24] C.R. He, W.G. Wang, Alumina doped Ni/YSZ anode materials for solid oxide fuel cells, Fuel Cells 9 (5) (2009) 630–635.
[25] S.Q. Fan, C.J. Li, C.X. Li, G.J. Liu, G.J. Yang, L.Z. Zhang, Preliminary study of performance of dye-sensitized solar cell of nano-TiO_2 coating deposited by vacuum cold spraying, Mater. Trans. 47 (7) (2006) 1703–1709.
[26] L.S. Wang, H.F. Zhou, K.J. Zhang, Y.Y. Wang, C.X. Li, X.T. Luo, G.J. Yang, C.J. Li, Effect of the powder particle structure and substrate hardness during vacuum cold spraying of Al_2O_3, Ceram. Int. 43 (5) (2017) 4390–4398.
[27] H.S. Ryu, T.S. Lim, J. Ryu, S.H. Hong, Corrosion protection performance of YSZ coating on AA7075 aluminum alloy prepared by aerosol deposition, J. Electrochem. Soc. 160 (1) (2013) C42–C47.
[28] C.W. Ahn, J.J. Choi, J. Ryu, B.D. Hahn, J.W. Kim, W.H. Yoon, J.H. Choi, D.S. Park, Microstructure and ionic conductivity in $Li_7La_3Zr_2O_{12}$ film prepared by aerosol deposition method, J. Electrochem. Soc. 162 (1) (2015) A60–A63.
[29] D.W. Lee, H.J. Kim, Y.N. Kim, M.S. Jeon, S.M. Nam, Substrate hardness dependency on properties of Al_2O_3 thick films grown by aerosol deposition, Surf. Coat. Technol. 209 (2012) 160–168.
[30] R.C. Dykhuizen, M.F. Smith, Gas dynamic principles of cold spray, J. Therm. Spray. Technol. 7 (2) (1998) 205–212.
[31] T. Schmidt, F. Gaertner, H. Kreye, New developments in cold spray based on higher gas and particle temperatures, J. Therm. Spray. Technol. 15 (4) (2006) 488–494.
[32] D.M. Chun, S.H. Ahn, Deposition mechanism of dry sprayed ceramic particles at room temperature using a nano-particle deposition system, Acta Mater. 59 (7) (2011) 2693–2703.
[33] S. Yin, X.F. Wang, X.K. Suo, H.L. Liao, Z.W. Guo, W.Y. Li, C. Coddet, Deposition behavior of thermally softened copper particles in cold spraying, Acta Mater. 61 (14) (2013) 5105–5118.
[34] A.G. Mamalis, I.N. Vottea, D.E. Manolakos, On the modelling of the compaction mechanism of shock compacted powders, J. Mater. Process Technol. 108 (2) (2001) 165–178.
[35] R. Prummer, Explosive compaction of powders, principle and prospects, Materwiss. Werksttech. 20 (12) (1989) 410–415.
[36] C.J. Li, A. Ohmori, Relationships between the microstructure and properties of thermally sprayed deposits, J. Therm. Spray. Technol. 11 (3) (2002) 365–374.
[37] M. Morales, J.J. Roa, J.M. Perez-Falcon, A. Moure, J. Tartaj, M. Segarra, Electrical and mechanical characterization by instrumented indentation technique of $La_{0.85}Sr_{0.15}Ga_{0.8}Mg_{0.2}O_{3-\delta}$ electrolyte for SOFCs, J. Eur. Ceram. Soc. 32 (16) (2012) 4287–4293.
[38] M. Morales, J.J. Roa, J.M. Perez-Falcon, A. Moure, J. Tartaj, E. Espiell, M. Segarra, Correlation between electrical and mechanical properties in $La_{1-x}Sr_xGa_{1-y}Mg_yO_{3-\delta}$ ceramics used as electrolytes for solid oxide fuel cells, J. Power Sources 246 (2014) 918–925.
[39] J.J. Choi, K.S. Cho, J.H. Choi, J. Ryu, B.D. Hahn, W.H. Yoon, J.W. Kim, C.W. Ahn, D.S. Park, J. Yun, Electrochemical effects of cobalt doping on (La,Sr)(Ga,Mg)$O_{3-\delta}$ electrolyte prepared by aerosol deposition, Int. J. Hydrog. Energ. 37 (8) (2012) 6830–6835.
[40] J.J. Choi, J.H. Choi, J. Ryu, B.D. Hahn, J.W. Kim, C.W. Ahn, W.H. Yoon, D.S. Park, Low temperature preparation and characterization of (La, Sr)(Ga, Mg)$O_{3-\delta}$ electrolyte-based solid oxide fuel cells on Ni-support by aerosol deposition, Thin Solid Films 546 (2013) 418–422.
[41] S.L. Zhang, T. Liu, C.J. Li, S.W. Yao, C.X. Li, G.J. Yang, M.L. Liu, Atmospheric plasma-sprayed $La_{0.8}Sr_{0.2}Ga_{0.8}Mg_{0.2}O_3$ electrolyte membranes for intermediate-temperature solid oxide fuel cells, J. Mater. Chem. A 3 (14) (2015) 7535–7553.
[42] C.S. Hwang, T.J. Hwang, C.H. Tsai, C.L. Chang, S.F. Yang, M.H. Wu, C.Y. Fu, Effect of plasma spraying power on LSGM electrolyte of metal-supported solid oxide fuel cells, Ceram. Int. 43 (2017) S591–S597.
[43] C.S. Hwang, C.H. Tsai, C.L. Chang, C.M. Chuang, Z.Y.C. Shie, S.W. Cheng, S.H. Wu, Plasma sprayed metal-supported solid oxide fuel cell and stack with nanostructured anodes and diffusion barrier layer, Thin Solid Films 570 (2014) 183–188.
[44] C.H. Lo, C.H. Tsai, C. Hwang, Plasma-sprayed YSZ/Ni-LSGM-LSCo intermediate-temperature solid oxide fuel cells, Int. J. Appl. Ceram. Technol. 6 (4) (2009) 513–524.
[45] M. Hrovat, A. Ahmad-Khanlou, Z. Samardzija, J. Holc, Interactions between lanthanum gallate based solid electrolyte and ceria, Mater. Res. Bull. 34 (12–13) (1999) 2027–2034.